THE JOURNAL OF PHYSICAL CHEMISTRY B

ARTICLE

pubs.acs.org/JPCB

Spectroscopic Study of the CP43′ Complex and the PSI−CP43′ Supercomplex of the Cyanobacterium *Synechocystis* PCC 6803

Ximao Feng,[†] Bhanu Neupane,[†] Khem Acharya,[†] Valter Zazubovich,[‡] Rafael Picorel,[§,∥] Michael Seibert,[§] and Ryszard Jankowiak*[,†]

[†]Department of Chemistry, Kansas State University, Manhattan, Kansas 66506, United States

[‡]Department of Physics, Concordia University, Montreal, Quebec, Canada

[§]National Renewable Energy Laboratory, Golden, Colorado 80401, United States

[∥]Estación Experimental de Aula Dei (CSIC), Zaragoza, Spain

Supporting Information

ABSTRACT: The PSI−CP43′ supercomplex of the cyanobacterium *Synechocystis* PCC 6803, grown under iron-starvation conditions, consists of a trimeric core Photosystem I (PSI) complex and an outer ring of 18 CP43′ light-harvesting complexes. We have investigated the electronic structure and excitation energy transfer (EET) pathways within the CP43′ (also known as the *isiA* gene product) ring using low-temperature absorption, fluorescence, fluorescence excitation, and hole-burning (HB) spectroscopies. Analysis of the absorption spectra of PSI, CP43′, and PSI−CP43′ complexes suggests that there are 13 chlorophylls (Chls) per CP43′ monomer, i.e., a number that was observed in the CP43 complex of Photosystem II (PSII) (Umena, Y. et al. *Nature* **2011**, *473*, 55−60). This is in contrast with the recent modeling studies of Zhang et al. (*Biochim. Biophys. Acta* **2010**, *1797*, 457−465), which suggested that IsiA likely contains 15 Chls. Modeling studies of various optical spectra of the CP43′ ring using the uncorrelated EET model (Zazubovich, V.; Jankowiak, R. *J. Lumin.* **2007**, *127*, 245−250) suggest that CP43′ monomers (in analogy to the CP43 complexes of the PSII core) also possess two quasi-degenerate low-energy states, A′ and B′. The site distribution functions of states A′ and B′ maxima/full width at half-maximum (fwhm) are at 684 nm/180 cm^{-1} and 683 nm/80 cm^{-1}, respectively. Our analysis shows that pigments mostly contributing to the lowest-energy A′ and B′ states must be located on the side of the CP43′ complex facing the PSI core, a finding that contradicts the model of Zhang et al. but is in agreement with the model suggested by Nield et al. (*Biochemistry* **2003**, *42*, 3180−3188). We demonstrate that the A′−A′ and B′−B′ EET between different monomers is possible, though with a slower rate than intramonomer A′−B′ and/or B′−A′ energy transfer.

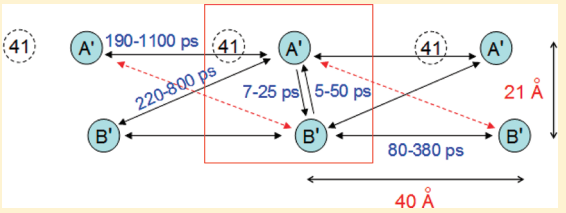

1. INTRODUCTION

Cyanobacteria account for more than half of the total photosynthetic productivity on Earth and can be found in almost every conceivable environment, including most marine and freshwater habitats.[1] One of the main reasons that cyanobacteria have become so ubiquitous is that their strong and effective regulatory mechanisms maintain high photosynthetic production levels under various conditions of illumination or nutrient stress.[2] Their adaptation to low-iron environments is an important example. When grown under iron-deficient conditions, the cyanobacterial phycobiliprotein content and Photosystem I (PSI) to Photosystem II (PSII) ratio are reduced. To compensate for this, some cyanobacteria express the *isiA* gene product. Multiple copies of chlorophyll a (Chl a) binding IsiA protein surround the PSI trimer to compensate for PSI content decreases under the iron-stress conditions.[3−5] This protein is a genetic homologue of PsbC, the CP43 protein of the PSII core, associated with the water-splitting and oxygen-evolving enzyme of photosynthesis. Therefore, it is often called CP43′.[4−6]

Although CP43 and CP43′ have high amino acid sequence homology, they show some key differences. Indeed, in addition to different mass due mainly to a marked shortening of the large E loop on the luminal side of CP43′, the His ligand that binds Chl 46 in CP43 is replaced with Gln in CP43′ of *Synechocystis* PCC 6803, and a Met residue, which has been implicated as a possible ligand in Chl 37 of CP43, is converted to a Phe in CP43′.[7] Both of these Chls have been suggested to play important roles in the excitation energy transfer (EET) dynamics of CP43, so comparison of the EET properties of these two protein complexes is of great interest.

A breakthrough in understanding the association of the proteins belonging to the core antenna family within the PSI core occurred a decade ago when two laboratories, using electron microscopy, discovered simultaneously that a supercomplex of trimeric PSI is encircled by a ring of 18 IsiA proteins in two

Received: June 27, 2011
Revised: October 5, 2011
Published: October 06, 2011

ACS Publications © 2011 American Chemical Society

different cyanobacterial species (*Synechocystis* PCC 6803[3,7] and *Synechococcus* PCC 7942[8]) when grown under limiting iron conditions. It has been established that while the whole PSI−CP43′ supercomplex has a diameter of 320 Å and a thickness of 90 Å each of the 18 CP43′ monomers has a width of about 24 Å and a 20° inclination relative to its neighbors.[9,10] Since then, much work has been dedicated to unraveling the spectroscopic properties and structure−function relationships in these complexes.[4,5,11−29]

The addition of the 18-mer CP43′ ring to PSI is an evolutionary adaptation to the reduction of the amounts of PSI and phycobilisomes under low-iron conditions, and it increases the light-harvesting efficiency of the PSI complexes by at least 70%.[3,4,7,8] Many studies using different spectroscopic methods have revealed that the CP43′ ring can transfer energy very effectively to the PSI core.[4,5,7,8] In addition, some groups have suggested that photoprotection of PSI (though PSI is not particularly prone to photodamage) and PSII under unfavorable environmental conditions might be the main function of the CP43′ complex.[18,21] Although significant progress has been made in our understanding of these complexes, many open issues remain. For example, the number of Chls constituting a CP43′ monomer is still under debate. It is most often assumed to be the same as the number of pigments present in the CP43 complex. However, the latter number has varied over time.[30−32] For example, in 2001, the 3.8 Å resolution X-ray structure of a cyanobacterial PSII core[30] revealed the presence of 12 Chl *a* molecules per CP43 monomer. In 2004, the crystal structure of a cyanobacterial PSII core complex at 3.5 Å resolution[31] suggested that each monomer has about 14 Chls. However, more recent structural data obtained at 3.0,[32] 2.9,[33] and 1.9 Å[34] resolutions, respectively, established that the number of Chls is 13. In contrast, ref 5 suggested 16−17 Chls per CP43′ monomer in another cyanobacterium (*Synechococcus* PCC 7942), while the modeling studies discussed in ref 10 proposed that each IsiA in the PSI−CP43′ supercomplex from the *Synechocystis* PCC 6803 binds 15 Chls. The latter value was obtained from calculations of optimal energy transfer within the PSI−CP43′ supercomplex.

In the present study, we show that each monomer of the CP43′ complex most likely possesses 13 Chls, in agreement with the number of pigments in CP43 of PSII,[32,34] and energy transfer between quasi-degenerate states with uncorrelated site distribution functions (successfully applied previously to explain the various optical spectra of CP43 of PSII[6,35]) can be used to explain the electronic structure and EET in the ring of the CP43′ complexes. Regarding the structure of the PSI−CP43′ supercomplex (i.e., the orientation of CP43′ monomers and the PSI trimer in relationship to each other), we argue below that our data are consistent with the model suggested by Nield et al.[9] and not with the model proposed recently by Zhang et al.[10]

2. EXPERIMENTAL SECTION

2.1. Sample Isolation Procedure. All glassware used for cell growth was first washed with dilute HCl (0.01 times commercial, concentrated HCl) to eliminate any iron adhering to the glass. A preculture of cyanobacteria at an optical density of about 1.0 (at 600 nm) was grown for two days in BG-11 mineral medium, lacking iron-containing compounds, and then it was diluted 15 times in the same medium to set the culture at an optical density of 0.1 (at 600 nm). The cultures were then grown for 21 days and harvested by centrifugation at 13 800*g* for 15 min at 4 °C. For the isolation of the CP43′ complex, *Synechocystis psaFJ*-depleted mutant cells[36] were used (this mutant synthesizes much lower amounts of PSI, thus reducing the risk of PSI contamination). Approximately 15 g cells (wet weight) were suspended in 50 mM MES−NaOH, pH 6.0, 25% (w/v) glycerol, 5 mM $CaCl_2$, and 5 mM $MgCl_2$ at a ratio of 10 mL of buffer per 1 g of cyanobacteria. The suspension was then centrifuged at 13 800*g* for 15 min at 4 °C; the pellet was suspended in the same original buffer volume with 1 mM PMFS (Sigma); and 50 μm/L of DNAase (Roche Diagnostics, Mannheim, Germany) was added. The cells were then broken by sonication (Ultrasonic Processor XL2020, Heat System) for 45 min. Cycles of 1 min and 30 s sonication and 1 min storage of the tubes on ice were employed to avoid sample overheating. The resultant cell extract was clarified by centrifugation at 121*g* for 5 min at 4 °C to eliminate any cell debris and large particles. The supernatant was finally centrifuged at 13 900*g* for 35 min at 4 °C, and the pellet contained thylakoid membranes.

2.2. Isolation of the CP43′ Complex. The above pellet was incubated with the same buffer (without PMFS and DNAase), supplemented with 1 M guanidinium chloride (GuCl) for 30 min at 4 °C, with gentle stirring to eliminate most of the phycobillisomes that contaminate the sample. The incubation was followed by a second centrifugation, and the resultant pellet was washed 1−2 more times under the same conditions until the supernatant was almost colorless. The final treated thylakoid membranes were resuspended in 20 mM bis-TRIS, pH 6.5, 10 mM $MgCl_2$, 20 mM NaCl, 15 mM $MgSO_4$, and 1.5% (w/v) taurine and then assayed spectrophotometrically for Chl *a* using an ε_{663nm} = 86 mM^{-1} cm^{-1} after pigment extraction with 80% (v/v) acetone.[37] The thylakoid membranes were next diluted to 0.15 mg of Chl/mL with the same buffer, treated with 1% (w/v) *n*-dodecyl β-D-maltoside (DM) for 1 h at 4 °C, and centrifuged at 9000*g* for 10 min at 4 °C. The resultant supernatant was loaded onto a weak anionic-exchange, DEAE (Toyopearl TSK DEAE 650s) column, pre-equilibrated with 20 mM bis-TRIS, pH 6.5, 10 mM $MgCl_2$, 20 mM NaCl, 15 mM $MgSO_4$, 1.5% (w/v) taurine, and 0.03% (w/v) DM. The bound green material was washed with about three column volumes of the same buffer and eluted with a 90−550 mM $MgSO_4$ continuous gradient in the same buffer. Fractions at around 250 mM $MgSO_4$ (2 mL each) with maxima at 671.5 nm (fractions with higher wavelength peaks contained some PSI core contamination as assayed by antibodies against the PSI core A protein subunit and were discarded) were saved and dialyzed overnight against 20 mM bis-TRIS, pH 6.5, 10 mM $MgCl_2$, 20 mM NaCl, 15 mM $MgSO_4$, 1.5% (w/v) taurine, and 0.01% (w/v) DM. After concentrating about 10 times with Centriprep tubes (30000 MWCO, Millipore), the sample was loaded onto a continuous sucrose gradient in buffer containing 20 mM bis-TRIS, pH 6.5, 10 mM $MgCl_2$, 20 mM NaCl, 15 mM $MgSO_4$, 1.5% (w/v) taurine, 0.01% DM, 0.5 M sucrose, and 4 M GuCl. To make the gradient, 10 mL of buffer solution (supplemented with 0.5 M sucrose) was put into ultracentrifuge tubes, frozen at −20 °C for at least 12 h, and then slowly thawed at 4 °C. This procedure formed a sucrose gradient with higher density sucrose at the bottom of the tubes. The concentrated sample from above was supplemented with 4 M GuCl; 0.5 mL of sample was loaded onto each tube; and the tubes were then centrifuged at 180 000*g* (SW 41Ti rotor, Beckman) for 6 h at 4 °C. Two main green bands were observed in the gradient. The band at higher density (faster mobility) was removed and dialyzed overnight against 20 mM bis-TRIS, pH 6.5, 10 mM $MgCl_2$, 20 mM NaCl,

15 mM $MgSO_4$, and 0.01% (w/v) DM. It had an absorption maximum at 671.5 nm. This preparation was then loaded onto a new DEAE 650s chromatography column, pre-equilibrated with the same dialysis buffer. Under these conditions CP43′ passed straight through the column, and it was subsequently loaded onto a Q-Sepharose (a strong anionic-exchange resin; GE Healthcare) column pre-equilibrated with 50 mM TRIS-HCl, pH 7.8, and 0.03% (w/v) DM. The column was washed with the same buffer and then with buffer supplemented with 50 mM $LiClO_4$. After washing, green material was eluted with a 50−300 mM $LiClO_4$ gradient in the same buffer. The fractions obtained at around 200 mM $LiClO_4$ were pooled and constituted the purified CP43′ complex. The room-temperature absorption maximum and the 77 K origin fluorescence band of pure CP43′ ring material were at 671.5 and 685 nm, respectively.

2.3. Isolation of the PSI−CP43′ Supercomplex. The isolation of the PSI−CP43′ supercomplex was performed as described above with some important modifications. Wild type *Synechocystis* PCC 6803 was used instead of the *psaFJ*-depleted mutant since the former contains much more PSI under iron-starvation conditions. Everything was done as explained before, except that only the fractions from the first DEAE column at around 350 mM $MgSO_4$ (with absorption peaks at around 673 nm) were collected, concentrated, and loaded onto the sucrose gradient tubes. After centrifugation, two main green bands were observed. The lower one was collected and dialyzed against buffer containing 20 mM bis-TRIS, pH 6.5, and 0.01% (w/v) DM. This sample constituted the PSI−CP43′ supercomplex, which had an absorption peak at 673 nm and two low-temperature fluorescence bands. The smaller fluorescence band was at 686 nm (due to CP43′), and the larger one was at 722 nm (due to PSI).

2.4. Spectroscopic Measurements. Details about the measurement setup were described elsewhere.[6,28] Here, only a brief description is given. A Bruker HR125 Fourier transform spectrometer was used to measure the absorption and hole-burning (HB) spectra. In absorption and nonresonant HB, the resolution was set at 4 cm^{-1}. For resonant HB, spectral resolution of 0.5 cm^{-1} was used. The fluorescence spectra were collected by a Princeton Instruments Acton SP-2300 monochromator equipped with a back-illuminated CCD camera (PI Acton Spec-10, 1340 × 400). All emission spectra were obtained with a resolution of 0.1 nm. The laser source for both nonresonant HB and fluorescence was 496.5 nm, produced from a Coherent Innova 200 argon ion laser. In the resonant HB and fluorescence excitation experiments, the tunable wavelengths came from a Coherent CR699 ring dye laser pumped by a Millenia 10s diode-pumped solid state laser at 532 nm from Spectra-Physics. With laser dye LD 688 (Exciton), the spectral range of 650−720 nm was available with a line width of 0.07 cm^{-1}. The power from the ring laser output was stabilized with a Laser Power Controller (Brockton Electro-Optics Corp.). The laser power in the experiments was precisely set by a continuously adjustable neutral density filter. All the experiments were performed at 5 K inside a Janis 8-DT Super Vari-Temp liquid helium cryostat. The sample temperature was read and controlled with a Lakeshore Cryotronic model 330 temperature controller. We emphasize that all nonphotochemical holes disappear after the annealing process, revealing an absorption spectrum identical to that prior to burning and thus proving that no irreversible photochemistry takes place. This is routinely verified by comparing the preburn absorption spectrum, and the spectrum collected after the sample was annealed to 150 K and cooled back to 5 K.

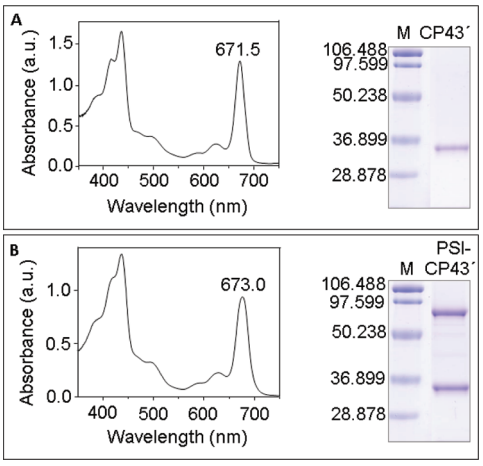

Figure 1. Room-temperature absorption spectra in the 350−750 nm spectral range and SDS-PAGE protein analysis of the CP43′ complex (Frame A) and the PSI−CP43′ supercomplex (Frame B) used in this study. M: molecular weight markers.

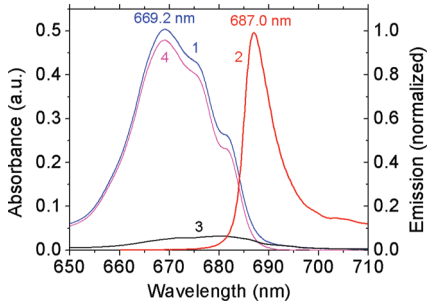

Figure 2. Q_y-region 5 K absorption (curve 1) and fluorescence (curve 2) spectra of isolated CP43′. Since curve 1 is partly (∼8−9%) contributed to by residual PSI (curve 3), curve 4 (4 = 1 − 3) represents the pure CP43′ absorption spectrum. Emission was obtained with an excitation wavelength (λ_{ex}) of 496.5 nm and an excitation laser intensity (I) of 100 $\mu W/cm^2$ (collection time 60 s).

3. RESULTS

3.1. Room-Temperature Absorption Spectra and SDS-PAGE of CP43′ and PSI−CP43′ Complexes. The room-temperature absorption spectrum of CP43′ in the 350−750 nm spectral range showed a maximum peak in the red at 671.5 nm (Figure 1A). Longer wavelength maxima indicate some contamination with the PSI complex, and a shorter maximum wavelength is an indication of the presence of some Chls disrupted from their native protein environment. The PSI−CP43′ supercomplex displayed a maximum in the red at around 673.0 nm (Figure 1B), due to the presence of the PSI trimer, which absorbs at a longer wavelength than CP43′. Note that the PSI−CP43′ 673.0 nm band is also much broader than that of the CP43′ complex. The SDS-PAGE (12% w/v acrylamide) protein analysis (Coomassie Blue staining) demonstrates the high purity of our preparations in terms of protein content. Indeed, the CP43′ complex contains only the IsiA polypeptide at around 34 kDa (Figure 1A), and the PSI−CP43′ preparation contains two main bands, one at around 34 kDa due to the IsiA protein and the other at around 66 kDa due to the PsaA and PsaB polypeptides of PSI (Figure 1B).

3.2. Low-Temperature Absorption and Emission Spectra. Absorption (curve 1) and emission (curve 2) spectra (T = 5 K) of isolated CP43′ rings are shown in Figure 2. The absorption spectrum with a maximum near 669.2 nm also shows two broad shoulders near 675 and 681−682 nm. This spectrum is similar to that obtained indirectly as a difference between the absorption spectra of the PSI−CP43′ supercomplex and the PSI trimeric core from *Synechocystis*.[28] However, the 675 and 681−682 nm bands were hardly visible in the 5 K absorption spectrum reported for the CP43′ complex from *Synechococcus* PCC 7942.[5] We also note that the intensity of the ∼681−682 nm shoulder is sample dependent and decreases in partly damaged samples.

Curve 1 in Figure 2, however, appears to possess a small contribution from the PSI trimer. That is, absorption in the long-wavelength region (>695 nm) originates exclusively from the PSI complex. To estimate the PSI contribution, the absorption spectrum of the PSI complex[28] (curve 3) was normalized with the CP43′ sample absorption spectrum (curve 1) in the 695−700 nm region. The difference spectrum (curve 4 = 1 − 3) corresponds to the absorption spectrum of "pure" (i.e., without PSI contamination) CP43′ complexes. The integrated area of curve 3 is only about 8−9% of spectrum 1. Thus, in the following analysis we assume that curve 4 is the absorption of the pure CP43′ complex. The emission spectrum (curve 2) in Figure 2 peaks at 687.0 nm with a fwhm of ∼7 nm, which is very similar to data reported in ref 18 for the CP43′ complex isolated from *Synechocystis* PCC 6803.

However, different emission peak positions have been observed for isolated CP43′ rings. For example, Andrizhiyevskaya et al.[5] observed a fluorescence origin band in CP43′ from *Synechococcus* near 682 nm, while the emission band was shifted to 685 nm in the PSI−CP43′ supercomplex. The authors of ref 5 attributed this shift to EET among the CP43′ monomers and/or pigment−pigment interactions between the monomers or between the CP43′ and PSI complexes in the PSI−CP43′ supercomplex. A 685 nm fluorescence band was also observed in CP43′ (*Synechocystis*) in ref 18. These PSI−CP43′ supercomplexes,[18] however, could lack some of the 18 CP43′ subunits normally present in intact supercomplexes. We will return to this issue in the modeling section (section 4.5) where the excitation energy transfer (EET) between quasi-degenerate low-energy states with uncorrelated site-distribution functions (SDFs)[6,35] within an individual CP43′ complex, and between the CP43′ subunits within the supercomplex, is discussed in detail. Here it is sufficient to say that our CP43′ and PSI−CP43′ complexes show emission bands with a maximum near 687 and 687/720 nm, respectively and that our 687 nm band and the 685 nm band from refs 26 and 28 have similar origins.

Figure 3 shows normalized (near 700 nm) 5 K absorption spectra of the PSI−CP43′ supercomplex (black; curve 1) and isolated PSI trimer sample[28] (blue; curve 2). Curve 3 is the difference between spectra 1 and 2 and is ascribed to the absorption spectrum of the pure CP43′ complex. As expected, the difference spectrum closely resembles curve 4 in Figure 2 (which is also seen in Figure 3 for easy comparison), proving that the isolated CP43′ ring and CP43′ residing within the PSI−CP43′ supercomplex have nearly indistinguishable absorption spectra.

3.3. Nonresonant Persistent and Transient Hole-Burned (HB) Spectra. The nonresonant HB spectra obtained with an excitation wavelength of 496.5 nm for the CP43′ complex are shown in Figure 4. The low-energy part of the absorption spectrum, which is similar to the absorption spectrum of CP43 of PSII,[6,38−40] is plotted for reference. Spectra labeled 1−8

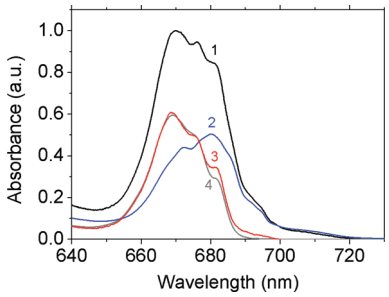

Figure 3. Absorption spectra (5 K) of the PSI−CP43′ supercomplex (black; curve 1) and PSI[28] (blue; curve 2) and their difference ascribed to pure CP43′ (curve 3). Curve 4 (gray spectrum) is shown for comparison and corresponds to spectrum 4 from Figure 2.

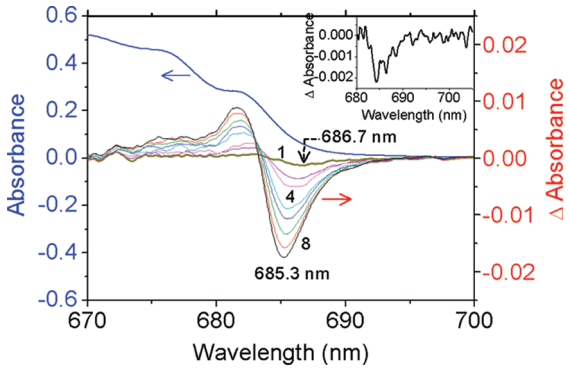

Figure 4. Mainframe shows the absorption spectrum (top) and HB spectra (labeled 1−8) obtained for the CP43′ complex at 5 K (λ_B = 496.5 nm). The fluences used for the shallow (curve 1) and saturated (curve 8) holes were 12 J/cm^2 and 7.7 kJ/cm^2, respectively. The inset shows the transient HB spectrum.

correspond to the nonresonant HB spectra. At very low fluence (f = 12 J/cm^2), a shallow hole (see curve 1) is observed at ∼686.7 nm with a hole depth of ∼2%. When this hole is saturated (see curve 8; f = 7.7 kJ/cm^2), the hole peak position shifts from 686.7 to 685.3 nm, and its depth increases to ∼17%. Fluence-dependent (blue-shifted) antiholes are also observed, in agreement with the nonphotochemical nature of persistent hole burning. Since contamination by the PSI trimer is very small, no persistent hole(s) typical of PSI trimer and/or PSI−CP43′ complexes are observed. Samples with a less intense ∼681−682 nm shoulder in absorption showed significantly blue-shifted nonresonant holes and emission spectra (data not shown). We will argue below that such behavior is consistent with a lack of efficient EET between subunits of the CP43′ supercomplex ring. The inset in Figure 4 shows a very shallow transient hole spectrum (hole depth of ∼1.3%; obtained with I = 600 mW/cm^2), which is the difference absorption spectrum generated with the laser on and with the laser off, measured after the persistent hole (see curve 8 in the mainframe) is saturated. The transient hole reflects the extent of the population accumulated at the triplet bottleneck state via intersystem crossing from the excited singlet state and is further discussed in section 4.6.

3.4. Fluence Dependence of the Emission Spectra. We turn now to fluorescence spectra obtained at different stages of nonresonant HB. All emission spectra in Figure 5 were obtained with low laser intensity (I = 100 μW/cm^2, integration time = 60 s). Spectrum 1 represents the emission of an unburned sample,

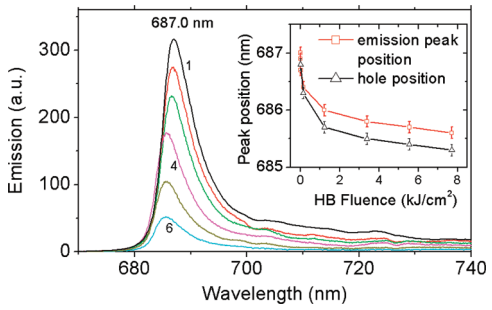

Figure 5. Fluorescence spectra (5 K) obtained with CP43′ at different stages of nonresonant hole burning. All emission spectra (labeled 1−6) were obtained with a laser excitation intensity of 100 μW/cm^2 (collection time 60 s). The inset shows the emission maxima (open circles) and nonresonant hole minima (open triangles) as a function of HB fluence. The excitation wavelength was 496.5 nm for both the HB and emission measurements.

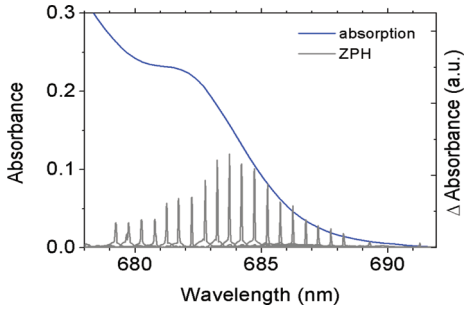

Figure 6. Solid curve is the corrected absorption spectrum of CP43′ from Figure 2 (curve 4). The gray sharp spikes correspond to an inverted ZPH action spectrum. The holes were burnt with a fixed fluence of 2.4 J/cm^2. See the text for details.

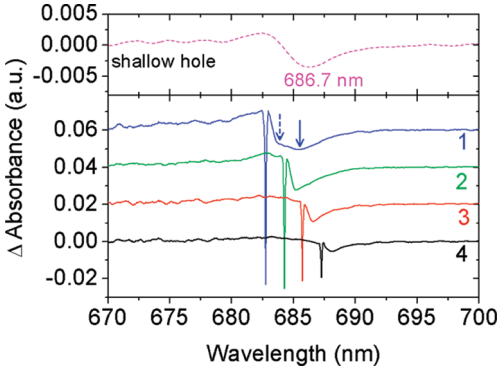

Figure 7. Spectra 1−4 are resonant HB spectra obtained for CP43′ complexes at 5 K. Four different λ_B's were used: 682.8 nm (1), 684.3 nm (2), 685.8 nm (3), and 687.3 nm (4). All spectra are offset vertically for clarity. The burn dose was 90 J/cm^2 for each spectrum (0.5 cm^{-1} resolution). The nonresonant (nonsaturated) HB spectrum (the pink dashed curve at the top, which is similar to curve 1 in Figure 4, and obtained with λ_B = 496.5 nm and a burn dose of 12 J/cm^2) is shown for comparison.

while spectra 2−6 were obtained after various stages of nonresonant HB, as shown in Figure 4. Curves 2−6 show that with increasing bleaching the integrated fluorescence intensity decreases, and the emission maximum shifts blue to about 686 nm. This is an indication that there are at least two states/pigments involved in the resulting emission, with somewhat different fluorescence yields. We believe that spectrum 1 in Figure 5 originates from the lowest-energy state(s) of intact CP43′ complexes. The position of the emission band near 687 nm does not depend on fluence as long as the fluence is kept lower than ~12 J/cm^2. The same emission maximum was measured for the intact PSI−CP43′ supercomplex (data not shown). However, in the latter case, due to an efficient EET to the PSI trimer, an additional strong band with a maximum near 720 nm was observed that originates from the PSI emission in agreement with refs 18 and 28 (electronic structure and EET dynamics of the PSI−CP43′ supercomplex will be discussed elsewhere). As mentioned above for the HB data, the blue shift of the emission upon burning can be explained assuming that the pigments contributing to the lowest-energy state are continuously burned and, on average, blue-shifted. Moreover, the resulting emission originates, to a progressively larger extent, from the low-energy state or states with modified composition (preferentially localized on Chl molecule(s) at different position within the complex). The nature of these low-energy states will be discussed below, as it is more complicated than in the case of the (monomeric) CP43[6] (due to the ring structure of the CP43′ complex where EET within a monomer subunit and between neighboring monomers must be possible). The inset in Figure 5 shows the position of the nonresonant hole (Figure 4) and the emission band (mainframe of Figure 5) as a function of fluence. Note that emission maxima shown in Figure 5 vary more or less in concert with the minima of the nonresonant holes as a function of HB fluence, and the largest shifts take place at the early stage of burning. Interestingly, similar dynamics of fluence-dependent emission are also observed in the PSII core and the CP47 complex from spinach.[41] The origin and shape of these fluorescence spectra are further discussed in section 4.

3.5. ZPH Action Spectrum and Nonresonantly Burnt Holes. To gain additional insight about the properties of the isolated CP43′ ring, we measured the zero-phonon hole (ZPH) action spectrum, which shows the dependence of the hole depth on the burn wavelength for a fixed burning dose.[28,42] It has been shown before[28] that this type of spectrum can resolve possible contributions to the lowest-energy states of photosynthetic complexes. The ZPH action spectrum (see inverted sharp peaks) of the CP43′ complex (obtained with a constant f = 2.4 J/cm^2) is presented in Figure 6. The depth of these holes is smaller than 10%, and the holes were burnt from long wavelength to short wavelength to reduce the contribution from the broad nonresonant low-energy holes. In Figure 6, however, the amplitudes of the holes were normalized to the low-energy wing of the absorption spectrum. The ZPH action spectrum has a maximum near 684 nm, which is about 2−3 nm blue-shifted in comparison to the shallow nonresonant hole shown in Figure 4 or the emission peak in Figure 5. The peak of the ZPH action spectrum is closer to the position of the saturated hole at 685.5 nm, suggesting that something besides the lowest-energy (very weak) 686.7 nm state contributes to the action spectrum under our experimental conditions.

To obtain more information about the nature of the lowest-energy states, we present the saturated resonant holes (obtained with a fluence of 90 J/cm^2) in Figure 7 (curves 1−4). The burning wavelengths for each of the four spectra are shown in the caption. Curve 4 is clearly composed of the ZPH and a pseudo-phonon sideband. Higher-energy excitations (curves 1 and 2) clearly reveal an additional contribution to the low-energy part of the hole structure (compare the different shapes/bandwidths of the low-energy holes) due to interference from the lowest-energy

state(s) bleached by downhill EET. Especially in the hole spectrum with λ_B = 682.8 nm (curve 1), one can see two apparent lower-energy components indicated by two vertical arrows. The shoulder (dashed arrow) near 683.8 nm (located about 20 cm^{-1} from the ZPH) corresponds to the pseudophonon sideband. The broader band near 685.3 nm (solid arrow) is due to downhill EET, in agreement with the 685.3 nm saturated hole obtained with an excitation of 496.5 nm (see curve 8 in Figure 4). This supports our earlier suggestion that the ZPH action spectrum shown in Figure 6 does not reflect exclusively the lowest-energy state(s). The top spectrum in Figure 7 (dashed line) is a shallow HB spectrum (similar to curve 1 in Figure 4). Note that its position is near 686.7 nm and likely corresponds to the lowest-energy state. Below we introduce a model of uncorrelated EET within the subunits of the CP43′ ring, which can be used to explain the above optical spectra obtained for the CP43′ ring.

4. DISCUSSION

4.1. Number of Chl *a* per CP43′ Subunit. The size of our PSI−CP43′ supercomplex particles, based on negative-staining TEM data obtained at NREL (data not shown), is consistent with the literature data;[3] i.e., a supercomplex studied in this work is composed of one PSI trimer and 18 CP43′ monomers. Assuming there are 288 Chls in the PSI core trimer and 18 copies of CP43′ encircling the PSI,[3,43] the approximate number of Chl *a* per CP43′ subunit can be derived by deconvoluting the absorption spectrum of the PSI−CP43′ supercomplex into CP43′ and PSI components, as shown in Figure 3. (All spectra were measured under identical conditions with 4 cm^{-1} resolution.) A comparison of the integrated absorption of the CP43′ (curve 3) and PSI (curve 2) spectra in Figure 3 reveals, assuming 18 CP43′ subunits per supercomplex,[3] that there are about 13 (±1) Chls in each CP43′ monomer (i.e., the same number of pigments as found in the CP43 complex of PSII).[32] Different numbers of pigments per CP43′ monomer were reported by different groups; for example, 10 Chl *a* per subunit were observed in ref 28 for *Synechocystis*, although comparison of the data from ref 28 with the spectra reported in the current work demonstrates (data not shown) that the CP43′ preparation studied in ref 26 was significantly contaminated with PSI complex; as a result, the number of Chls was underestimated. By the same token, results for *Synechococcus*,[5] in which the Chl *a* content was estimated at 17−18, could be explained assuming that the number of CP43′ subunits is higher than 18 per PSI trimer. Formation of a second CP43′ ring around the first one has been observed in the case of prolonged iron stress.[26]

4.2. On the Relative Orientation of Chls in the CP43′ Ring with Respect to the PSI Trimer: Structural Considerations. The available models of the PSI−CP43′ supercomplex are inferred from crystal structures of PSI and the CP43′ protein.[9,10] As structural data on CP43′ per se are yet unavailable, the CP43′ (IsiA) is modeled on the basis of a high-resolution crystal structure of CP43,[30] an antenna protein of PSII that is homologous with IsiA.[44,45] The current understanding of the mutual arrangement of CP43′ and PSI core complexes is based on relatively low-resolution (25 Å) electron microscopy data,[7] which allows for considerable freedom in orienting CP43′ subunits in relation to the PSI core. As a result, two mutually exclusive models exist. In the one by Nield et al.[9] the CP43′ subunits are oriented with the same side toward the core as CP43 is oriented with respect to the RC in PSII. Twelve Chls were included in the original Nield et al. model,[9] which was based on the result given by the low-resolution X-ray structure of PSII.[30] Later studies showed that CP43 may be associated with 13 or even 14 Chls.[31,32] The highest resolution X-ray data so far, however, reveal only 13 Chls per CP43 monomer.[34] This is in contrast with the recent work of Zhang and co-workers,[10] who suggest that the CP43′ protein binds 15 Chls. Moreover, in Zhang's model the opposite side of the CP43′ subunit is facing the PSI core. This model is based on theoretical optimization of the energy transfer pathways in the PSI−CP43′ supercomplex. Below, we will refer to the models of Nield et al.[9] and Zhang et al.,[10] as models I and II, respectively. Although Zhang et al.[10] argued that model II is superior to model I with respect to the energy transfer potential (i.e., more Chls and Chl−Chl connections and increased number of paths along which EET occurs[10]), model II appears to be inconsistent with many optical spectra obtained so far for CP43.[6,38−40,46,47] For example, it has been shown that the CP43 core antenna complex of PSII possesses two quasi-degenerate "red"-trap states, A and B.[6,38−40,46,47] The evidence for similar lowest-energy states in CP43′ has been presented by us in ref 28. For CP43, a model of uncorrelated EET between the quasi-degenerate bands has been proposed,[6,35] which is consistent with both experimental results and excitonic calculations.[48] The latter reveal that Chl 44 and Chl 37 (using Loll et al. notation[32]) are most likely contributing to the low-energy A and B states, respectively, in the CP43 complex.[48] From the viewpoint of optimizing EET from CP43′ to the PSI core under these conditions, Chls 44 and 37 should face the PSI core (model I), as the opposite CP43′ orientation would result in poor antenna performance. Therefore, in subsequent analysis, model I will be used, as this model provides orientation of Chls consistent with the spectroscopic data and previous modeling studies.[6,48]

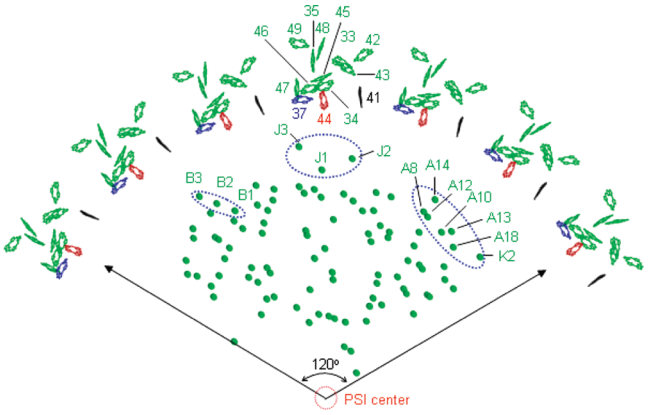

Figure 8. Pigment organization in the PSI−CP43′ supercomplex proposed by Nield et al.[9] with an extra Chl added (Chl 47) based on ref 32. The notation for the PSI pigments is given based on ref 43. For clarity, only part of the supercomplex is shown. The view is from the lumenal side. Blue, red, and black Chls correspond to Chls 37, 44, and 41, respectively. See the text for details.

Figure 8 illustrates relative positions of the Chls in model I with the 13th pigment (Chl 47) added based on the higher-resolution crystal structure at 3.0 Å of PSII.[32,49] The pigments are numbered according to PDB file 2AXT. The Chls in PSI and CP43′ are represented by the Mg atoms (green circles) and chlorin rings, respectively. The blue-dotted ovals show regions where PSI pigments have the nearest distances to the CP43′ pigments,

possibly involved in funneling excitation energy from CP43′ subunits to the PSI trimer. Note that in this structural arrangement Chls 37, 44, and 41 face the PSI complex. Chl 41 is located at the edge of the CP43′ monomer and close to the adjacent CP43′ monomer. Chl 37 and Chl 44 transition dipoles are 12° and 20° off the membrane plane, with their molecular planes perpendicular and almost parallel to the supercomplex radius, respectively. The Chl 41 transition dipole is 29° off the membrane plane, and its molecular plane is also parallel to the supercomplex radius. Model II,[10] with clearly labeled Chls, is shown in Figure S1 of the Supporting Information for the convenience of readers. In model II each CP43′ monomer is associated with 15 Chls, with Chls 37, 41, and 44 placed on the exterior of the PSI−CP43′ supercomplex (i.e., far from the CP43′−PSI interface). It is interesting to note that Chl 41 (close to the RC of PSII in the case of CP43), according to model I, is located close to a neighboring CP43′ subunit in the ring. Hence, it could act as a linker in the intersubunit (i.e., intermonomer) EET within the CP43′ ring. It is this *intermonomer* EET that should account for the differences observed in the CP43′ emission and persistent/transient HB spectra (i.e., the red-shift) in comparison to CP43, as illustrated below.

4.3. Uncorrelated EET Model within the CP43′ Ring. As mentioned above, a model of the energy transfer between quasi-degenerate states with uncorrelated SDFs has been successfully applied to characterize the two lowest-energy states in CP43.[6,35] In this model, SDFs of the two Chl molecules (i.e., pigments A and B) contributing to the lowest-energy absorption band of CP43 are uncorrelated, but the respective molecules are connected by relatively fast (∼10 ps) excitation energy-transfer processes. In a given CP43 complex, either of these two Chls could be lower in energy.[35] In the following discussion "pigments A and B" are going to be used as a shorter way of referring to pigments having dominant contribution to states A and B, and "bands A and B" are meant to represent absorption bands belonging to states A and B, respectively. The important feature of this model is that it explains the asymmetric shape of the HB action spectrum resulting from its being a superposition of the sub-SDF of the pigments A and B, which are the lowest-energy pigments in the individual complexes. These sub-SDF contributions to the action spectrum are red-shifted with respect to the true full SDF of the pigments A and B. States A and B of CP43 are assumed to be highly localized on Chls 44 and 37, respectively, with interpigment coupling of 5.8−7.6 cm^{-1}. Note that both of these states possess some excitonic character (as evidenced by CD and Stark-SHB data[39,40] and excitonic calculations[48]) but are preferentially localized on a lower site-energy pigment in a respective group. The possible reason(s) for the significant red shift in the transition frequency of the Chls contributing to the A and B bands could be due to H-bonding and/or different ligation state with protein environment.[48] In the following, we employ this EET model, with modifications accounting for the differences between the CP43 monomer and the CP43′ ring, to find out whether the optical spectra reported in section 3 can be explained. Specifically, with the CP43′ ring, one needs to consider the EET between *neighboring* CP43′ monomers. In the CP43 complex (as discussed in refs 6 and 35), one of the two lowest-energy pigments (A or B) can only transfer energy to the other lowest-energy pigment (B or A) in the same CP43 unit. In contrast, in the CP43′ ring composed of 18 subunits (CP43′ monomers), each CP43′ unit is located at a very close distance (∼10 Å) with respect to its two neighbors, and energy transfer

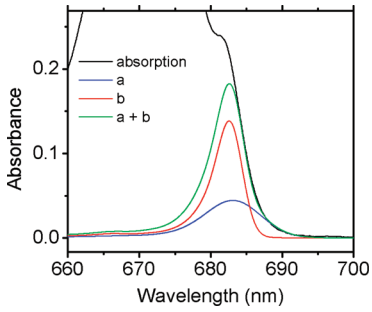

Figure 9. Fit of the long-wavelength region of the absorption of CP43′, with contributions from the two lowest-energy states: curve a for band A′ (peak at 684 nm with fwhm of 180 cm^{-1}) and curve b for band B′ (peak at 683 nm with fwhm of 80 cm^{-1}) dressed with phonons and vibrations.

between them is likely to occur.[9,10] In the case of CP43′, we refer to A′ and B′ pigments to distinguish from A and B pigments of the CP43 complex. Therefore, in this case, every A′ pigment (of an individual subunit) has up to five potential energy acceptors (i.e., the B′ pigment of the same CP43′ monomer as well as two A′ pigments and two B′ pigments of the two adjacent monomers). Similarly, every B′ pigment has up to five potential acceptors (i.e., the A′ pigment of the same CP43′ monomer as well as two B′ pigments and two A′ pigments of the adjacent monomers). Taking the above into account in the following subsections, we describe the model most suitable for the CP43′ protein and verify whether one set of parameters can simultaneously fit the absorption, emission, persistent/transient holes, and ZPH action spectra of the CP43′ ring.

4.4. Absorption Spectrum of the Isolated CP43′ Protein. Figure 9 shows the CP43′ absorption spectrum from Figure 2 corrected for PSI contamination (black curve). Curves a and b in Figure 9 are absorption spectra of states A′ and B′, respectively, including contributions from delocalized protein phonons and localized Chl vibrations (according to Rätsep et al.[50]). For the best fit, we used the Huang−Rhys factor, $S = 0.6$, which is about two times larger than that in the analysis for CP43.[6] Considering maximal depths of the saturated ZPH (∼42%) in Figure 7, the estimated upper limit for S could be as large as 0.8. The oscillator strength of the A′ band is 0.6 Chl equivalents. This is in agreement with the results of ref 6, where we did not explicitly report this number, although it was available. The oscillator strength of the B′ band is slightly larger than one Chl equivalent, again in implicit agreement with ref 6. Note that the low-energy part of the absorption spectrum can be fit very well with the sum of curves a and b. From the fit, parameters of possible SDFs of the A′ and B′ bands can be extracted. We note that somewhat different bandwidths and band positions can also yield a good fit to the low-energy wing of this absorption spectrum. However, the range of possible SDF parameters needs to be narrowed considerably to describe all experimental data reported above, including the emission and action spectra, as well as nonresonantly burned holes. That is, the best parameters revealed by our modeling studies (including those described in detail in the next section) are the SDF of band A′ ($SDF_{A'}$), which peaks at 684.0 nm and has a fwhm of 180 cm^{-1}, and the SDF of band B′ ($SDF_{B'}$), which peaks at 683.0 nm with a fwhm of 80 cm^{-1}. Interestingly, these two states have similar parameters to those previously reported for CP43′, where the two bands were found with absorption peaks/inhomogeneous widths of 683.9 nm/160 cm^{-1} and 682.6 nm/70 cm^{-1}, respectively.[28] In that study,

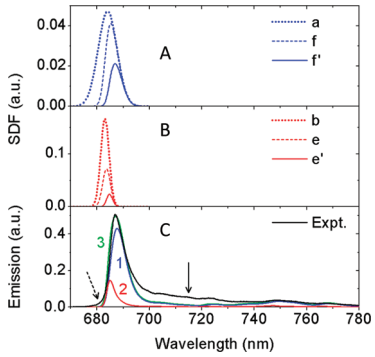

Figure 10. (Frame A) Curve a corresponds to the true SDF of band A′ in CP43′. Curves f and f ′ represent the subensembles of band A′, without and with intermonomer EET taken into account, respectively. (Frame B) Curve b corresponds to the true SDF of band B′. Curves e and e′ represent subensembles of band B′, without and with intermonomer EET taken into account, respectively. (Frame C) Emission spectrum of the CP43′ protein at 5 K (black curve). Curve 3 is the sum of curves 1 and 2 (corresponding to contributions of f′ and e′ from frames A and B, respectively) dressed with phonons and localized Chl vibrations. For details about the discrepancy indicated by the dashed and solid arrows, see the main text.

however, information about these two bands had been obtained indirectly by fitting the CP43′ ZPH action spectrum, in turn obtained as a difference between the ZPH action spectra of PSI−CP43′ and PSI complexes. Compared with parameters reported for CP43 (A band: 682.9 nm/180 cm^{-1}; B band: 682.9 nm/62 cm^{-1}),[6] the CP43′ complex appears to have a red-shifted A′ band. This difference is reasonable if one takes into consideration slight differences in the protein sequence between CP43 and IsiA complexes.

4.5. Emission Spectrum of Isolated CP43′ Protein. The SDF profiles, derived from data shown in Figure 9, are (in a good approximation) the full "true" SDFs of the two lowest-energy pigments in CP43′. They are plotted in frames A and B of Figure 10, as curves a and b, respectively. In a particular CP43′ complex, either one of the two pigments could be lower in energy. In contrast to the absorption spectrum, where both the higher- and lower-energy sides are based on the "true" SDFs of the A′ and B′ bands, in isolated CP43 or CP43′ subunits, the emission and ZPH action spectra are mainly contributed to by the subensembles of the two lowest-energy pigments, which are the lowest-energy pigments in their respective individual complexes and are incapable of further downhill EET. The SDFs for these subensembles of A′ (or B′) in CP43′ can be calculated by multiplying the "true" SDF, a (or b), by the respective probabilities that pigments with zero-phonon lines (ZPLs) at certain wavelengths are incapable of any downhill EET, that is, by the normalized integration curve of the "true" SDFs.[6,35] The resulting distributions are represented by curves f and e for bands A′ and B′, respectively.

To expand this discussion to *intermonomer* EET within the CP43′ ring, one has to consider the likelihood of various intermonomer EET processes (A′−A′, B′−B′, A′−B′, B′−A′). Note that the diameters of the PSI−CP43′ supercomplex and CP43′ monomer are 320 and 48 Å, respectively.[3,9,10] In the ring composed of 18 CP43′ units, each monomer has a 20° tilt relative to its neighbors. Therefore, the distances between identical Chl molecules in neighboring CP43′ monomers are about 40 Å. The shortest Chl−Chl distance between neighboring CP43′ monomers is, however, only about 10 Å.[9] Furthermore, using Chl

Table 1. Couplings (in cm^{-1}) between Relevant Chl a Molecules (Model I) within and between Adjacent CP43′ Subunits[a]

		Monomer 1			Monomer 2		
		Chl 37	Chl 41	Chl 44	Chl 37	Chl 41	Chl 44
Monomer 1	Chl 37	0	1.52	5.74	−1.77	0.09	0.02
	Chl 41	1.52	0	−16.72	−1.06	1.11	−2.55
	Chl 44	5.74	−16.72	0	−1.03	−0.29	1.10
Monomer 2	Chl 37	−1.77	−1.06	−1.03	0	1.52	5.74
	Chl 41	0.09	1.11	0.29	1.52	0	−16.72
	Chl 44	0.02	−2.55	1.10	5.74	−16.72	0

[a] μ^2 = 18.5 D.

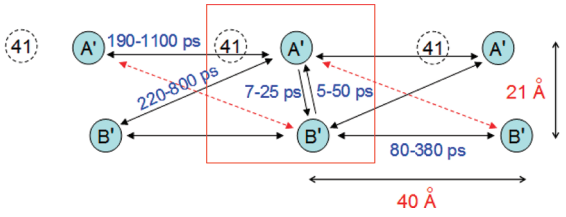

Figure 11. Schematic diagram of possible EET pathways within a single monomer and between monomers (i.e., intermonomer EET) viewed from inside the supercomplex in the membrane plane. Pigments A′ and B′ most likely represent Chls 44 and Chls 37, respectively, with Chls 41 acting as a possible linker in intermonomer A′−A′ energy transfer. The red box shows the boundary of one CP43′ monomer. Some typical EET times and distances are also shown.

coordinates from the X-ray structure of PSII (PDB 2AXT[32]), the distance between Chl 44 and Chl 37 inside a monomer is about 23 Å, compared to about 45 Å between Chl 37 and 44 pigments of two neighboring monomers. The interpigment couplings, for pigments relevant within the structural Model I, are presented in Table 1. We note that in this range of couplings Förster approximation must be valid. Figure 11 presents a schematic diagram of pigment locations and expected EET times in three neighboring CP43′ monomers out of the 18-unit ring as viewed from the PSI trimer. In this figure, for clarity, only Chl molecules corresponding to the two lowest-energy states in a CP43′ monomer (Chl 44 for state A′ and Chl 37 for state B′), and the possible Chl 41 energy transfer linker between two CP43′ monomers, are plotted. The EET rates shown in Figure 11 have been calculated based on the Förster mechanism using realistic spectral overlap integrals between Chl 37 and Chl 44.[51] The overlap integral dependence on the donor−acceptor ZPL gap is calculated numerically based on the actual shape of the single-site spectra with the experimentally determined phonon sideband (PSB) and local mode parameters. All parameters in these calculations are the same as in our previous CP43 study,[6] except that to achieve good fits of various optical spectra for the CP43′ ring we used the slightly larger S value of 0.6 as discussed above. Note that one of the intermonomer A′−B′ processes is significantly more likely than the other one and exhibits a rate comparable to the A′−A′ intermonomer rate. The intermonomer B′−B′ EET rate is still larger, due to both higher coupling and better spectral overlap. Most of these times (except for one of the A′−B′ processes) are short enough compared to the fluorescence lifetime of several nanoseconds, and respective EET processes

are expected to reduce the hole burning and fluorescence yields of the donor pigments, according to

$$\text{1st eq. for } \phi_{fl}(\tau_{EET}) = \frac{\tau_{fl}^{-1}}{\tau_{fl}^{-1} + \tau_{EET}^{-1}} \text{ and } \phi_{NPHB}(\tau_{EET})$$

and

$$\text{2nd eq. for } \phi_{NPHB} = \frac{\Omega_0 \exp(-2\lambda)}{\Omega_0 \exp(-2\lambda) + \tau_{fl}^{-1} + \tau_{EET}^{-1}}$$

Here, $\phi_{NPHB}(\tau_{EET})$ is the NPHB yield; $\phi_{fl}(\tau_{EET})$ is the fluorescence yield; $\Omega_0 \exp(-2\lambda)$ is the NPHB rate; τ_{fl} is the fluorescence lifetime; and τ_{EET} is the EET time.

When intermonomer EET is taken into consideration, each of the A′ and B′ pigments can transfer to several acceptors (one in the same monomer and three in its neighboring monomers). Therefore, sub-SDF of the pigments incapable of downhill EET due to the absence of any further acceptors are shifted to the longer-wavelength region, as illustrated by curves f′ and e′ in Figures 10A and 10B, respectively. Note that both of these curves peak at wavelengths significantly longer than the true SDFs (i.e., curves a and b), and only these bands dressed with phonons and localized chlorophyll vibrations should contribute to the emission spectra. The fit of the emission spectrum with the origin band at 687 nm is shown in frame C of Figure 10. Curves 1 and 2 in frame C of Figure 10 are curves f′ and e′ from frames A and B, respectively, dressed with delocalized protein phonons and localized Chl vibrations. Again, $S = 0.6$ is a realistic value based on the upper limit for S (∼0.8) estimated from the maximal depths of saturated resonant holes (∼42%), especially when PSI contamination partly contributes to the absorption near 685 nm (and is poorly burnable). The above contributions fit the emission spectrum reasonably well, assuming the relative contribution from band 2 (red), as discussed above, is reduced by a factor of 3 in comparison with the intensity of contribution from band 1 (blue). This reduction is in line with observations presented in Figure 5, where upon burning and blue-shifting of higher fluorescence yield A′-type pigments, the relative weight of lower fluorescence yields B′-type pigments in emission increases, and the overall emission decreases. Small changes of the S factor and/or shape of the phonon sideband did not significantly affect the calculated emission spectrum. Agreement between the calculated and experimental spectra, for such a complex system, is remarkably good, although small discrepancies at both high- and low-energy spectral regions still exist. First, it appears, in agreement with the spectral analysis shown in Figure 2, that the measured emission spectrum contains a small contribution from the broad PSI core emission, indicated by the solid arrow (PSI core emission maximum lies near 722 nm, fwhm = 22 nm[26]). On the whole, the emission spectrum can be fitted assuming 7−10% of PSI contamination, which is in agreement with our earlier conclusion that contamination of PSI is estimated to be about 8−9% of the CP43′ absorption in our isolated preparations (see Figure 2). On the other hand, the small discrepancy between the calculated and experimental emission spectra on the high-energy side (dashed arrow in Figure 10C) could be due to emission coming from pigments with some EET channels unavailable to them, possibly due to damage beyond "normal" static disorder. As a result, their emission should be blue-shifted, in agreement with the measured emission spectra of partly damaged complexes (data not shown). Recall that previously reported fluorescence maxima of CP43′ complexes varied from 682 to 687 nm.[5] In the framework of the model presented here, the exact position of the fluorescence maximum will depend on the intactness of the intermonomer EET pathways.

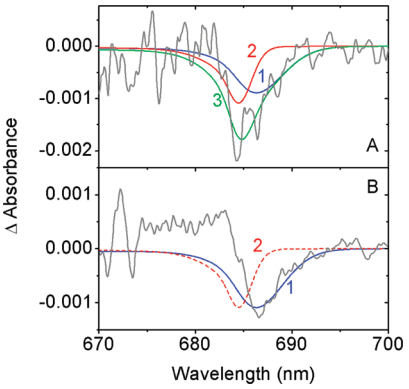

Figure 12. (Frame A) Fit of the transient hole spectrum (noisy curve) with SDFs of subensembles of the two lowest-energy states, f′ and e′, dressed with phonons and localized Chl vibrations (curves 1 and 2, respectively). Curve 3 is the sum of curves 1 and 2. (Frame B) Fit of the persistent hole spectrum obtained at low fluence (noisy curve) with the SDF of the subensemble of one of the two lowest-energy states, f′, dressed with phonons and localized Chl vibrations (curves 1); see text for details.

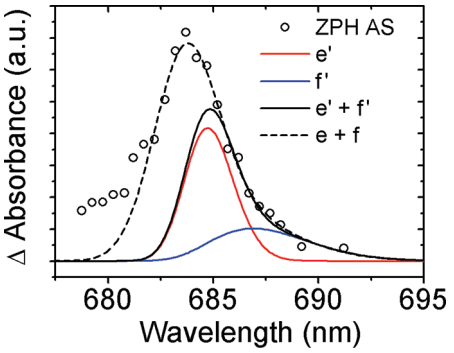

Figure 13. Fit of the high-dose ZPH action spectrum (ZPH AS; open circles) of CP43′ with subensemble SDFs of the two lowest-energy states (A′ and B′) without intermonomer EET (curves f and e) and with intermonomer EET (curves f′ and e′).

4.6. Nonresonant Persistent and Transient Holes. The gray curves in frames A and B of Figure 12 show transient (see inset of Figure 4) and shallow persistent (curve 1 from Figure 4) nonresonant HB spectra of CP43′, respectively. The gray spectrum in frame B reflects the lowest-energy substate(s), as discussed above. Although both experimental curves are very noisy, due to extreme shallowness of the holes (i.e., ∼1%), the spectra can be fitted using our EET model discussed above. That is to say, the transient spectrum in frame A of Figure 12 can be described by the two lowest-energy states, f′ (curve 1) and e′ (curve 2), dressed with phonons and localized Chl vibrations. Curve 3 is the sum of curves 1 and 2. The long-wavelength region of the persistent hole in frame B of the same figure is also in agreement with the shape of the f′ band (curve 1); the contribution from the e′ band (dashed curve) cannot be assessed in this case due to interference from an antihole, a typical feature observed in persistent hole spectra,[35,39] although it appears that state f′ contributes more during the early stage of HB, in agreement with data shown in Figures 4 and 5.

4.7. Analysis of the ZPH Action Spectrum. Figure 13 shows the ZPH action spectrum of CP43′ with hole depths (from Figure 6) plotted as open circles. Recall that, if all relevant EET

processes in the CP43′ ring (intermonomer and intramonomer) are very fast, the ZPH action spectrum would be described only by the sum (weighted by the HB yield) of bands f′ and e′ from Figure 10. This is clearly not the case. Note, however, that curves f′ and e′ discussed above are consistent with the long-wavelength region of the ZPH action spectrum. To obtain a good fit (black solid curve) to the lower-energy side of the action spectrum, the original curve e′ needs to be multiplied by a factor of 3 (see red solid curve). Apparently, as in the case of the CP43 complex,[6] the HB yield of the B′ band in CP43′ is about three times higher than in the A′ band. The discrepancy between the solid black curve and the high-energy region of the action spectrum implies that intermonomer EET is relatively slow, in agreement with data in Figure 11. That is, for long EET times (e.g., hundreds of ps; see Figure 11) pigments described by (e minus e′) and (f minus f′) may also experience SHB, though at a slower rate than fractions of pigments described by bands f′ and e′, truly incapable of the downhill EET. The dashed line represents the theoretical ZPH action spectrum when contributions (e′ minus e) and (f′ minus f) are taken into account. This argument becomes even more convincing if one notes that the HB action spectrum was measured with 2.4 J/cm^2 and at 0.5 cm^{-1} resolution. Thus, the holes were in fact much deeper than the apparent 10%, and the (e minus e′) and (f minus f′) fractions were clearly probed alongside e′ and f′ fractions. One cannot also exclude that, since the action spectrum was measured from lower to higher energies, some antihole absorption (exhibiting high HB/recovery yields) was added at 680−684 nm, while burning was performed at longer wavelengths.

4.8. Structural Implications. As shown in ref 9, the PSI−CP43′ supercomplex contains 18 CP43′ monomers in a ring around the PSI trimer. However, in vivo the ring is not perfect due to distortions arising from the PSI trimer exhibiting C_3 symmetry. In each PSI monomer, there are three regions where PSI Chls are situated within 20−25 Å of the Chls in CP43′ monomers, as shown by the three blue-dashed ovals in Figure 8. Only these molecules are likely energy acceptors that can receive excitation energy from the CP43′ antenna ring and then transfer it to the reaction center of the PSI. Similarly, not all CP43′ monomers have the same likelihood of transferring energy directly to the PSI because of their nonequivalent positions relative to the PSI energy acceptors. Therefore, in addition to the lowest-energy states in each single CP43′ monomer, one should consider the lowest-energy states that constitute minima among several neighboring CP43′ monomers. It appears that pigments responsible for such global lowest-energy states should be relatively close to the above-mentioned PSI acceptors, as this would ensure the most effective excitation energy transfer. One could speculate that C_3-type distortion to the CP43′ ring can cause compression of monomers in certain positions within the ring, with associated additional red shift of the lowest-energy pigments. (This selective compression of course will not occur in the isolated CP43′ ring.) This mechanism could focus excitation energy toward the desired regions of the PSI core.

5. CONCLUSIONS

From a comparative study of various absorption spectra of PSI−CP43′, CP43′, and PSI complexes, we conclude that, in samples studied in this work, there are about 13 Chls in each of the 18 CP43′ monomers in the PSI−CP43′ supercomplex. The latter is in perfect agreement with the number of pigments observed in CP43 of PSII.[32,34] By analyzing the absorption, emission, persistent/transient HB spectra, as well as the ZPH action spectrum of CP43′ using the modified uncorrelated EET model,[6,35] we suggest, by analogy with the CP43 complex, that there appear to be two nearly degenerate lowest-energy states (with a dominant contribution from pigments A′ and B′) in each monomer. That is, the above states are mostly localized on single pigments. The states, A′ and B′, have site distribution functions peaking at 684.0 nm (fwhm of 180 cm^{-1}) and 683.0 nm (fwhm of 80 cm^{-1}), respectively. We argue that within each monomer EET between these two quasi-degenerate states occurs. From the fit of the red-shifted emission spectrum, it is clear that EET must also take place among the CP43′ monomers. This is in good agreement with descriptions of nonresonant transient and persistent holes, as discussed above. Both analysis of the HB action spectrum and direct calculation of intermonomer transfer times indicate that the latter are relatively long. For optimal energy transfer in the PSI−CP43′ supercomplex, it would be useful if the CP43′ monomers possessing the lowest-energy pigments among the neighboring subunits were aligned with the regions of the PSI cores having spatially and energetically optimized pigments. These monomers could then efficiently transfer excitation energy, funneled from other CP43′ monomers, to the PSI core. Finally, assuming that CP43 and CP43′ monomers have similar structures, which is consistent with high amino acid homology between the two proteins, our data support the structural model (regarding the orientation of CP43′ complexes within the ring surrounding the PSI core) proposed by Nield et al.[9] This view is in agreement with our previous modeling studies[6] and excitonic calculations for the CP43 complex of PSII, where we argued that most likely pigments contributing to the lowest A and B states are Chl 44 and Chl 37, respectively. A combination of CP43′ relative orientation according to Nield et al.[9] with the above assignment of the two lowest-energy pigments of CP43′ could facilitate very efficient energy transfer from the antenna CP43′ complexes to the PSI reaction center.

■ ASSOCIATED CONTENT

Supporting Information. For completeness, a rival pigment organization of the PSI−CP43′ supercomplex, as recently proposed by Zhang et al.,[10] including pigment labeling (not provided in the original paper) is shown in Figure S1. This material is available free of charge via the Internet at http://pubs.acs.org.

■ AUTHOR INFORMATION

Corresponding Author
*E-mail: ryszard@ksu.edu.

■ ACKNOWLEDGMENT

This work was supported by the NSF ARRA Grant (CHE-0907958). V.Z. acknowledges support by NSERC, R.P. by MICINN (Grant AGL2008-00377) in Spain, and M.S. by the US Department of Energy's Photosynthetic Systems Program within the Chemical Sciences, Geoscience, and Biosciences Division of the Office of Basic Energy Sciences under NREL Contract #DE-AC36-08-GO28308. We also acknowledge helpful discussions with Mike Reppert (Department of Chemistry, MIT) and TEM studies conducted by Bryan Donohue (NREL).

REFERENCES

(1) Stewart, I.; Falconer, I. R. In *Oceans and human health: risks and remedies from the seas*; Wash, P. J., Smith, S. L., Fleming, L. E., Eds.; Academic Press: New York, 2008; pp 271−296.

(2) Grossman, A. R.; Schaefer, M. R.; Chiang, G. G.; Gollier, J. L. In *The Molecular Biology of Cyanobacteria*; Bryant, D. A., Ed.; Kluwer Academic Publishers, Dordrecht, 1994; pp 487−517.

(3) Bibby, T. S.; Nield, J.; Barber, J. *Nature* **2001**, *412*, 743–745.

(4) Melkozernov, A. N.; Bibby, T. S.; Lin, S.; Barber, J.; Blankenship, R. E. *Biochemistry* **2003**, *42*, 3893–3903.

(5) Andrizhiyevskaya, E. G.; Schwabe, T. M. E.; Germano, M.; D'Haene, S.; Kruip, J.; van Grondelle, R.; Dekker, J. P. *Biochim. Biophys. Acta* **2002**, *1556*, 265–272.

(6) Dang, N. C.; Zazubovich, V.; Reppert, M.; Neupane, B.; Picorel, R.; Seibert, M.; Jankowiak, R. *J. Phys. Chem. B* **2008**, *112*, 9921–9933.

(7) Bibby, T. S.; Nield, J.; Barber, J. *J. Biol. Chem.* **2001**, *276*, 43246–43252.

(8) Boekema, E. J.; Hifney, A.; Yakushevska, A. E.; Piotrowski, M.; Keegstra, W.; Berry, S.; Michel, K. P.; Pistorius, E. K.; Kruip, J. *Nature* **2001**, *412*, 743–745.

(9) Nield, J.; Morris, E. P.; Bibby, T. S.; Barber, J. *Biochem.* **2003**, *42*, 3180–3188.

(10) Zhang, Y.; Chen, M.; Church, W. B.; Lau, K. W.; Larkum, A. W. D.; Jermiin, L. S. *Biochim. Biophys. Acta* **2010**, *1797*, 457–465.

(11) Sandström, S.; Ivanov, A. G.; Park, Y. -Y.; Öquist, G.; Gustafsson, P. *Physiol. Plant* **2002**, *116*, 255–263.

(12) Kouřil, R.; Yeremenko, N.; D'Haene, S.; Yakushevska, A. E.; Keegstra, W.; Matthijs, H. C. P.; Dekker, J. P.; Boekema, E. J. *Biochim. Biophys. Acta* **2003**, *1607*, 1–4.

(13) Andrizhiyevskaya, E. G.; Frolov, D.; van Grondelle, R.; Dekker, J. P. *Biochim. Biophys. Acta* **2004**, *1656*, 104–113.

(14) Aspinwall, C. L.; Duncan, J.; Bibby, T.; Mullineaux, C. W.; Barber, J. *FEBS Lett.* **2004**, *574*, 126–130.

(15) Michel, K. -P.; Pistorius, E. K. *Physiol. Plant* **2004**, *120*, 36–50.

(16) Sarcina, M.; Mullineaux, C. W. *J. Biol. Chem.* **2004**, *279*, 36514–36518.

(17) Dekker, J. P.; Boekema, E. J. *Biochim. Biophys. Acta* **2005**, *1706*, 12–39.

(18) Ihalainen, J. A.; D'Haene, S.; Yeremenko, N.; van Roon, H.; Arteni, A. A.; Boekema, E. J.; van Grondelle, R.; Matthijs, H. C. P.; Dekker, J. P. *Biochemistry* **2005**, *44*, 10846–10853.

(19) Kouřil, R.; Arteni, A. A.; Lax, J.; Yeremenko, N.; D'Haene, S.; Rögner, M.; Matthijs, H. C. P.; Dekker, J. P.; Boekema, E. J. *FEBS Lett.* **2005**, *579*, 3253–3257.

(20) Elli, A. F.; Jelezko, F.; Tietz, C.; Studier, H.; Brecht, M.; Bittl, R.; Wrachtrup, J. *Biochem.* **2006**, *45*, 1454–1458.

(21) Ivanov, A. G.; Krol, M.; Sveshnikov, D.; Selstam, E.; Sandström, S.; Koochek, M.; Park, Y. -I.; Vasil'ev, S.; Bruce, D.; Öquist, G.; Huner, N. P. A. *Plant Physiol.* **2006**, *141*, 1436–1445.

(22) Murray, J. W.; Duncan, J.; Barber, J. *Trands Plant Sci.* **2006**, *11*, 1360–1385.

(23) Singh, A. K.; Sherman, L. A. *Photosynth. Res.* **2007**, *93*, 17–25.

(24) van der Weij-de Wit, C. D.; Ihalainen, J. A.; van de Vijver, E.; D'Haene, S.; Matthijs, H. C. P.; van Grondelle, R.; Dekker, J. P. *Biochim. Biophys. Acta* **2007**, *1767*, 1393–1400.

(25) Stork, T.; Michel, K. -P.; Pistorius, E. K.; Dietz, K. −J. *J. Exp. Bot.* **2005**, *56*, 3193–3206.

(26) Yeremenko, N.; Kouřil, R.; Ihalainen, J. A.; D'Haene, S.; van Oosterwijk, N.; Andrizhiyevskaya, E. G.; Keegstra, W.; Dekker, H. L.; Hagemann, M.; Boekema, E. J.; Matthijs, H. C. P.; Dekker, J. P. *Biochemistry* **2004**, *43*, 10308–10313.

(27) Chen, M.; Bibby, T. S. *Photosynth. Res.* **2005**, *86*, 165–173.

(28) Riley, K. J.; Zazubovich, V.; Jankowiak, R. *J. Phys. Chem. B* **2006**, *110*, 22436–22446.

(29) Berera, R.; van Stokkum, I. H. M.; D'Haene, S.; Kennis, J. T. M.; van Grondelle, R.; Dekker, J. P. *Biophys. J.* **2009**, *96*, 2261–2267.

(30) Zouni, A.; Witt, H. -T.; Kern, J.; Fromme, P.; Kraub, N.; Saenger, W.; Orth, P. *Nature* **2001**, *409*, 739–743.

(31) Ferreira, K. N.; Maghlaoui, T. M.; Barber, J.; Iwata, S. *Science* **2004**, *303*, 1831–1838.

(32) Loll, B.; Kern, J.; Saenger, W.; Zouni, A.; Biesiadka, J. *Nature (London, U.K.)* **2005**, *438*, 1040–1044.

(33) Guskov, A.; Kern, J.; Gabdulkhakov, A.; Broser, M.; Zouni, A.; Saenger, W. *Nat. Struct. Mol. Biol.* **2009**, *16*, 334–342.

(34) Umena, Y.; Kawakami, K.; Shen, J. −R.; Kamiya, N. *Nature* **2011**, *473*, 55–60.

(35) Zazubovich, V.; Jankowiak, R. *J. Lumin.* **2007**, *127*, 245–250.

(36) Jeanjean, R.; Zuther, E.; Yeremenko, N.; Havaux, M.; Matthijs, H. C. P.; Hagemann, M. *FEBS Lett.* **2003**, *549*, 52–56.

(37) Porra, R. J.; Thompson, W. A.; Kriedemann, P. E. *Biochim. Biophys. Acta* **1989**, *975*, 384–394.

(38) Groot, M.; Frese, R. N.; de Weerd, F. L.; Bromek, K.; Pettersson, Å.; Peterman, E. J. G.; van Stokkum, I. H. M.; van Grondelle, R.; Dekker, J. P. *Biophys. J.* **1999**, *77*, 3328–3340.

(39) Jankowiak, R.; Zazubovich, V.; Rätsep, M.; Matsuzaki, S.; Alfonso, M.; Picorel, R.; Seibert, M.; Small, G. J. *J. Phys. Chem. B* **2000**, *104*, 11805–11815.

(40) Hughes, J. L.; Picorel, R.; Seibert, M.; Krausz, E. *Biochemistry* **2006**, *45*, 12345–12357.

(41) Neupane, B.; Dang, N. C.; Acharya, K.; Reppert, M.; Zazubovich, V.; Picorel, R.; Seibert, M.; Jankowiak, R. *J. Am. Chem. Soc.* **2010**, *132*, 4214–4229.

(42) Reddy, N. R. S.; Picorel, R.; Small, G. J. *J. Phys. Chem.* **1992**, *96*, 6458–6464.

(43) Jordan, P.; Fromme, P.; Witt, H. T.; Klukas, O.; Seanger, W.; Kruss, N. *Nature (London, U.K.)* **2001**, *411*, 909–917.

(44) Zhang, L.; McSpadden, B.; Pakrasi, H. B.; Whitmarsh, J. *J. Biol. Chem.* **1992**, *267*, 19054–19059.

(45) La Roche, J.; Boyd, P. W.; McKay, R. M. L; Gelder, R. J. *Nature* **1996**, *382*, 802–805.

(46) Di Donato, M; van Grondelle, R; van Stokkum, I. H.; Groot, M. L. *J. Phys. Chem. B* **2007**, *111*, 7345–7352.

(47) de Weerd, F. L.; van Stokkum, I. H. M.; van Amerongen, H.; Dekker, J. P.; van Grondelle, R. *Biophys. J.* **2002**, *82*, 1586–1597.

(48) Reppert, M.; Zazubovich, V.; Dang, N. C.; Seibert, M.; Jankowiak, R. *J. Phys. Chem. B* **2008**, *112*, 9934–9947.

(49) Müh, F.; Renger, T.; Zouni, A. *Plant Physiol. Biochem. (Issy les Moulineaux, Fr.)* **2008**, *46*, 238–264.

(50) Rätsep, M.; Pieper, J.; Irrgang, K. -D.; Freiberg, A. *J. Phys. Chem. B* **2008**, *112*, 110–118.

(51) Herascu, N.; Najafi, M.; Amunts, A.; Pieper, J.; Irrgang, K. -D.; Picorel, R.; Seibert, M.; Zazubovich, V. *J. Phys. Chem. B* **2011**, *115*, 2737–2747.